Laguerre-based method for analysis of time-resolved fluorescence data: application to *in-vivo* characterization and diagnosis of atherosclerotic lesions

Javier A. Jo
University of California — Davis
Department of Biomedical Engineering
Davis, California 95616

Qiyin Fang
McMaster University
Department of Engineering Physics
Hamilton, Ontario, Canada

Thanassis Papaioannou
Cedars-Sinai Medical Center
Department of Surgery
Los Angeles, California

J. Dennis Baker
Amir H. Dorafshar
Todd Reil
University of California Los Angeles
David Geffen School of Medicine
Department of Vascular Surgery
Los Angeles, California

Jian-Hua Qiao
Michael C. Fishbein
University of California Los Angeles
David Geffen School of Medicine
Department of Pathology and Laboratory Medicine
Los Angeles, California

Julie A. Freischlag
Johns Hopkins University
School of Medicine
Baltimore, Maryland

Laura Marcu
University of California — Davis
Department of Biomedical Engineering
Davis, California 95616
E-mail: lmarcu@bmsrs.usc.edu

Abstract. We report the application of the Laguerre deconvolution technique (LDT) to the analysis of *in-vivo* time-resolved laser-induced fluorescence spectroscopy (TR-LIFS) data and the diagnosis of atherosclerotic plaques. TR-LIFS measurements were obtained *in vivo* from normal and atherosclerotic aortas (eight rabbits, 73 areas), and subsequently analyzed using LDT. Spectral and time-resolved features were used to develop four classification algorithms: linear discriminant analysis (LDA), stepwise LDA (SLDA), principal component analysis (PCA), and artificial neural network (ANN). Accurate deconvolution of TR-LIFS *in-vivo* measurements from normal and atherosclerotic arteries was provided by LDT. The derived Laguerre expansion coefficients reflected changes in the arterial biochemical composition, and provided a means to discriminate lesions rich in macrophages with high sensitivity (>85%) and specificity (>95%). Classification algorithms (SLDA and PCA) using a selected number of features with maximum discriminating power provided the best performance. This study demonstrates the potential of the LDT for *in-vivo* tissue diagnosis, and specifically for the detection of macrophages infiltration in atherosclerotic lesions, a key marker of plaque vulnerability. [DOI: 10.1117/1.2186045]

Keywords: Laguerre deconvolution; fluorescence spectroscopy; optical diagnosis; vulnerable atherosclerotic plaques.

Paper 05194SSR received Jul. 18, 2005; revised manuscript received Dec. 1, 2005; accepted for publication Dec. 1, 2005; published online Mar. 27, 2006.

1 Introduction

Laser-induced fluorescence spectroscopy (LIFS) has been extensively explored as a technique for detecting biochemical changes in tissue due to pathological conditions, including cancer and atherosclerosis.[1–8] A central task in the development of LIFS-based diagnosis systems is designing a computational framework for processing the fluorescence signal and assessing the tissue composition. Such framework includes algorithms for 1. identifying and extracting features from the fluorescence signal that best reflect the tissue composition; and 2. combining these fluorescence-derived features for tissue classification. Ultimately, such algorithms are to be embedded into the LIFS instrumentation to provide automated,

Address all correspondence to Laura Marcu, Biomedical Engineering, University of California — Davis, Genome and Biomedical Sciences Bldg., 451 E. Health Sciences Dr., Davis, CA 95616. Tel: 530–752–0288. Fax: 530–754–5739. E-mail: lmarcu@ucdavis.edu

1083-3668/2006/11(2)/021004/13/$22.00 © 2006 SPIE

real-time, and accurate diagnostic information to clinicians.

Most of the applications of LIFS to tissue diagnosis have been developed for steady-state domain,[2–7] where features retrieved from fluorescence emission spectrum are correlated to tissue composition. Although the fluorescence spectrum provides a wealth of information about the tissue biochemistry, the steady-state measurements are sensitive to intensity artifacts, tissue absorption and scattering distortion, and excitation-collection geometry variation. In contrast, time-resolved (TR) fluorescence measurements are related to the submillisecond decay properties of the fluorophore lifetime and are insensitive to intensity variations. Thus, TR measurements are more robust and more suitable for clinical applications, where the presence of endogenous absorbers (i.e., hemoglobin) and intensity artifacts (i.e., probe/tissue movement) cannot be fully controlled.

Recently, we reported a new deconvolution method for the analysis of TR-LIFS data, in which the intrinsic fluorescence decay is estimated using a nonparametric expansion on an orthonormal Laguerre basis.[9] The Laguerre deconvolution technique presents a number of advantages over conventional multiexponential methods, including the linearization of the fitting parameters and faster convergence, and the potential of providing quantitative information about tissue biochemical composition.[9] In this study, the performance of the Laguerre deconvolution is evaluated in TR-LIFS measurements taken *in vivo* from rabbit aortas. In addition, the derived Laguerre expansion coefficients are investigated as a new domain for representing TR-LIFS data.

A number of classification algorithms have been tested for steady-state LIFS-based tissue diagnosis. Principal component analysis (PCA) and multivariate linear discriminant analysis (LDA) have been applied in LIFS-guided angioplasty and detection of cervical cancer.[10,11] Artificial neural networks (ANN) were designed to analyze autofluorescence of peripheral vascular tissue.[12,13] More advanced methods, including Bayesian and radial basis function networks and support vector machines, have been applied to the diagnosis of cervical and nasopharyngeal carcinomas.[14,15] On the contrary, very few studies have explored classification algorithms for TR-LIFS-based diagnosis. In this work, we present the application of multivariate statistical methods to the analysis of TR-LIFS data, and evaluate the potential of this approach for assessing the biochemical composition of atherosclerotic plaques. Due to the limited sample size available, this study focused on the more elementary algorithms of LDA, PCA, and feed-forward ANN.

Atherosclerotic plaque composition is an important predictor for plaque rupture. Plaque rupture and subsequent thrombosis are the most frequent underlying cause of acute coronary events and sudden death.[16] Rupture typically occurs at the lesion edges rich in mononuclear inflammatory cells,[17–19] including macrophage/foam cells.[20,21] Consequently, techniques capable of detecting macrophages *in vivo* will be instrumental to assess the risk of plaque complication. Previous studies have characterized the emission spectra of the main fluorescence components of the arterial wall (elastin, and various collagen and lipids types).[1] A few other studies have reported the application of LIFS to the identification of plaque disruption,[22] detection of plaques with thin fibrous caps,[23] and discrimination of lipid-rich lesions.[1] Nevertheless, to the best of our knowledge, the *in-vivo* detection of macrophages in atherosclerosis using LIFS has not been reported.

In this study, a computational framework for TR-LIFS based diagnosis was developed. Fluorescence measurements were obtained *in vivo* from normal and atherosclerotic rabbit aorta, and analyzed to evaluate: 1. the performance and robustness of the Laguerre deconvolution technique for *in-vivo* applications; 2. the applicability of the Laguerre expansion coefficients as features reflecting tissue composition; and 3. the performance of several classification algorithms for the diagnosis of atherosclerosis.

2 Methods

2.1 *Animal Model and Experimental Procedure*

Eight male New Zealand white rabbits (10 to 15 lbs body weight) were included in this study. Each rabbit was fed a high cholesterol diet for at least eight weeks prior to study. The experimental procedure involved exposing the intimal luminal surface of the rabbit aorta, and obtaining TR-LIFS measurements from areas visually identified as either normal or atherosclerotic. After spectroscopic investigations, the interrogated arterial segments were removed for histological analysis. A detailed description of the animal model and experimental protocol has been described in detail elsewhere.[24,25]

2.2 *Time-Resolved Laser-Induced Fluorescence Spectroscopy Instrumentation*

The experiments were conducted with a TR-LIFS prototype system, recently developed by our group and previously described.[26] Briefly, artery autofluorescence was induced with a pulsed nitrogen laser (wavelength 337 nm, pulse width 700 ps). Laser excitation output measured at the tip of the probe was set at 2 μJ/pulse.[27] Excitation and collection were performed via a bifurcated fiber optic probe. The collected autofluorescence was dispersed by an imaging spectrometer/monochromator, and detected with a gated multichannel plate photomultiplier tube (rise time 180 ps). The autofluorescence was temporally resolved using a digital oscilloscope (bandwidth 1 GHz, sampling rate 5 Gsamples/s) coupled to a preamplifier (bandwidth 1.5 GHz).

2.3 *Time-Resolved Laser-Induced Fluorescence Spectroscopy In-Vivo Measurements*

TR-LIFS measurements were obtained with serial scanning of the monochromator across the spectral range of 360 to 600 nm, in increments of 5 nm. The total acquisition time across the scanned emission spectrum was about 37 s. After acquisition of each time-resolved fluorescence spectrum, the laser pulse temporal profile was measured at a wavelength slightly below the excitation laser line. This profile was used as the input signal (system response) in the deconvolution algorithm to estimate the intrinsic fluorescence decays.

2.4 *Histological Analysis*

Following *in-vivo* TR-LIFS measurements, the aortic segments were removed, fixed, processed routinely, and evaluated microscopically by two cardiovascular pathologists. Each sample was characterized based on its overall histopathology (normal versus atherosclerotic lesion), intima thickness (thin

versus thick), and biochemical composition (collagen-rich versus macrophage-rich). A lesion was defined as thin if the intima thickness was less than 50 μm, or as thick otherwise. A collagen-rich lesion was defined as having collagen content greater than 50% and macrophage content less than 20%. A macrophage-rich lesion was defined as having macrophage content larger than 20% and collagen content smaller than 50%. Overall, the following five categories were identified: 1. normal artery (normal), 2. thin collagen-rich lesion (thin-collagen), 3. thin macrophage-rich lesion (thin-mac), 4. thick collagen-rich lesion (thick-collagen), and 5. thick macrophage-rich lesion (thick-mac).

2.5 *Time-Resolved Laser-Induced Spectroscopy Data Analysis*

The arterial TR-LIFS measurements were processed using the Laguerre deconvolution technique (LDT). This nonparametric method expands the intrinsic fluorescence decay or impulse response function (FIRF) on the discrete time Laguerre basis.[9,28] The Laguerre functions (LF) form an orthonormal basis with a built-in exponential term that makes them suitable for modeling physical systems with asymptotically exponential relaxation dynamics.[29] Due to the LF's orthogonality, LDT can reconstruct FIRFs of arbitrary form, providing a unique and complete expansion of the decay function.

In the context of time-domain TR-LIFS, the measured fluorescence intensity decay data $y(n)$ can be expressed as the (discrete) convolution of the FIRF $h(n)$ with the system response $x(n)$[9,30]:

$$y(n) = T \cdot \sum_{m=0}^{K-1} h(m)x(n-m), \quad n = 0, \ldots, K-1. \tag{1}$$

The parameter K in Eq. (1) is the number of data samples, while T is the sampling interval. LDT uses the orthonormal set of discrete time LF $b_j^{\alpha}(n)$ to expand the FIRF:

$$h(n) = \sum_{j=0}^{L-1} c_j b_j^{\alpha}(n). \tag{2}$$

In Eq. (2), c_j are the unknown Laguerre expansion coefficients (LEC), $b_j^{\alpha}(n)$ denotes the j'th order orthonormal discrete time LF, and L is the number of LFs used to expand the FIRF.[9,29] The LF basis is defined as:

$$b_j^{\alpha}(n) = \alpha^{(n-j)/2}(1-\alpha)^{1/2} \sum_{k=0}^{j} (-1)^k \binom{n}{k} \binom{j}{k} \alpha^{j-k}(1-\alpha)^k, \quad n \geq 0. \tag{3}$$

The Laguerre parameter ($0 < \alpha < 1$) determines the rate of exponential decline of the LF. Thus, FIRF with a longer lifetime will require a larger α value for efficient representation.[9,29] By inserting Eq. (2) into Eq. (1), the convolution Eq. (1) becomes:

$$y(n) = \sum_{j=0}^{L-1} c_j \nu_j(n),$$

$$\nu_j(n) = T \sum_{m=0}^{K-1} b_j^{\alpha}(m)x(n-m). \tag{4}$$

In Eq. (4), $\nu_j(n)$ are the discrete time convolutions of the system response $x(n)$ with the LF of order j. Finally, the unknown expansion coefficients can be estimated by the generalized linear least-square solution of Eq. (4) using the measured discrete signals $y(n)$ and $\nu_j(n)$. The number of Laguerre functions and the α value were chosen to minimize the normalized mean square error (NMSE) and secure the randomness in the estimation residuals. To assure this, L was changed from 1 to 6 and α from 0.6 to 0.9, and LDT was applied using each combination of these parameters to all the measured data. NMSE and the 95% confidence interval for random independent residuals were inspected for each L-α combination in all datasets. Optimal values of L=4 Laguerre functions and α=0.88 were determined.

Once the FIRF was estimated for each emission wavelength, the steady-state spectrum (I_λ) was computed by integrating each $h(n)$ as a function of time. To characterize the temporal dynamics of each fluorescence decay, three sets of parameters were estimated: 1. the average lifetime ($\tau_{f-\lambda}$), computed as the interpolated time at which the FIRF decays to 1/e of its maximum value; 2. the time constants ($\tau_{1-\lambda}$ and $\tau_{2-\lambda}$) and the relative amplitude ($A_{1-\lambda}$) from a biexponential model of the FIRF; and 3. the normalized value of the corresponding LECs ($c_{j-\lambda}, j=0, \ldots, L-1$). Therefore, a complete characterization of the fluorescence TR spectrum for each investigated aortic segment was given by the variation of these spectroscopic parameters $\{I_\lambda, \tau_{f-\lambda}, \tau_{1-\lambda}, \tau_{2-\lambda}, A_{1-\lambda}$, and $c_{j-\lambda}\}$ as a function of emission wavelength λ_E.

2.6 *Statistical Analysis*

A univariate statistical analysis (one-way analysis of variance, ANOVA) was used to compare the parameters $\{I_\lambda, \tau_{f-\lambda}, \tau_{1-\lambda}, \tau_{2-\lambda}, A_{1-\lambda}$, and $c_{j-\lambda}\}$ at specific λ_E's for each category of aortic segments as defined by histopathology. A post-hoc comparison test (Student-Newman-Keuls) was used to complement the results of the ANOVA test. A p-value of <0.05 was assumed to indicate statistical significance. Results of this statistical analysis provided a semiempirical evaluation of those spectroscopic parameters likely to provide discrimination among the different histopathological categories. All the results are presented as mean ± standard error (SE).

2.7 *Classification Methods*

Three linear classification algorithms were investigated: linear discriminant analysis (LDA),[10,31] stepwise linear discriminant analysis (SLDA), and principal component analysis (PCA).[10,11,32] A nonlinear classifier, the feed-forward neural network (FFNN), was also evaluated.[12,13,31] Based on the statistical analysis described before, three different sets of TR-LIFS parameters were selected and defined as: 1. spectral (SP: ratios of I_λ), 2. TR Laguerre (LAG: values/ratios of $c_{j-\lambda}$), and 3. TR biexponential (BEXP: values of $\tau_{1-\lambda}, \tau_{2-\lambda}, A_{1-\lambda}$) features. Based on the histopathological categories defined in the previous sections, two classification criteria were applied. Classification 1 was designed to discriminate normal, thick-

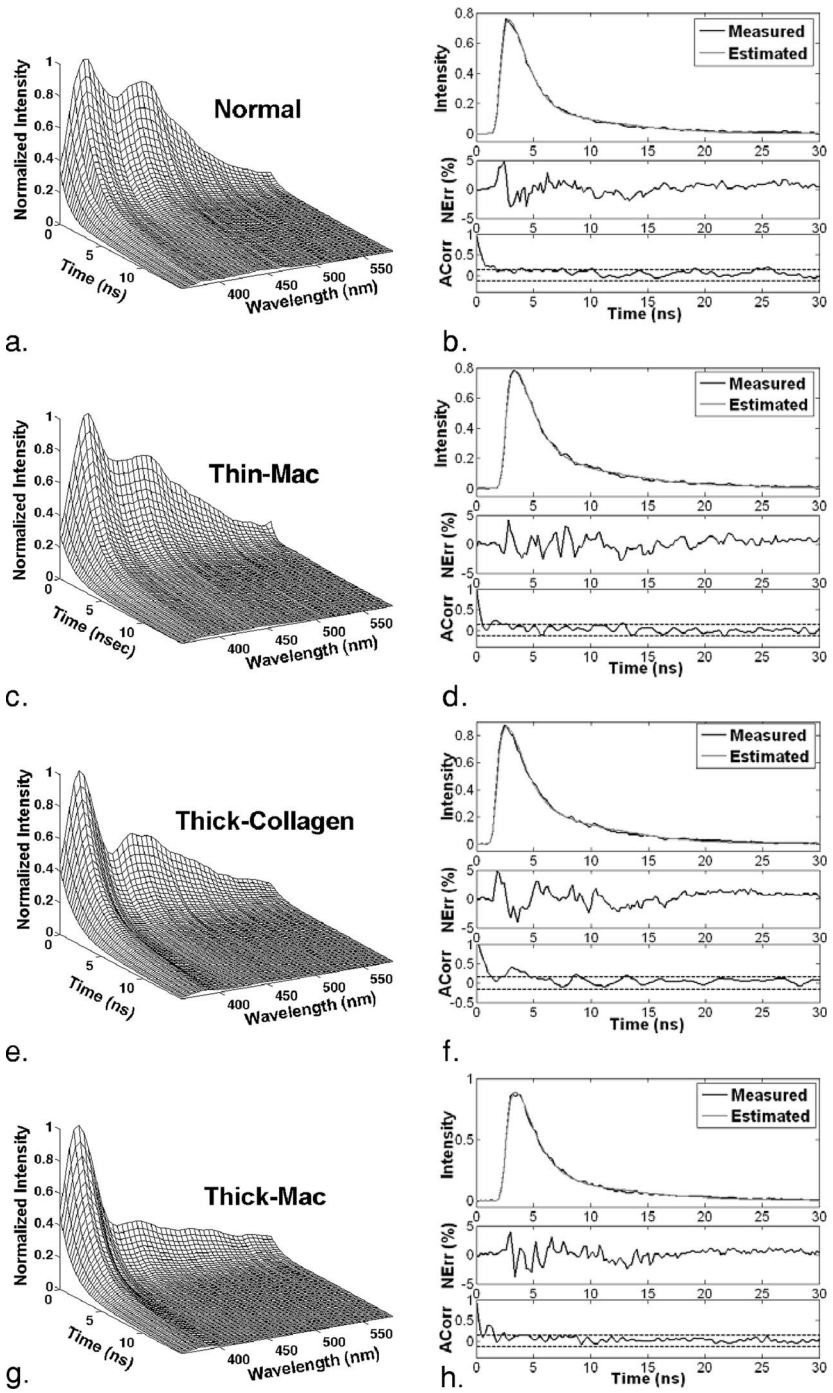

Fig. 1 Representative time-resolved fluorescence spectra, measured and estimated decays (at 390 nm), and the corresponding normalized error (NErr) and autocorrelation function (ACorr) for: (a) and (b) normal, (c) and (d) thin-mac, (e) and (f) thick-collagen, and (g) and (h) thick-mac.

collagen, and thick-mac specimens. Classification 2 was designed to distinguish normal, thin-collagen, and thin-mac specimens. These two criteria were used to evaluate the performance of the different feature types and classification algorithms.

2.7.1 *Linear classification algorithm*

Given an initial feature space, linear discriminant analysis (LDA)[10,31] aims to find an optimal transformation to map the original feature vectors into a lower-dimensional space that best discriminates among classes. Such an optimal transformation minimizes the within-class statistical distance and simultaneously maximizes the between-class statistical distance. The resulting mapping is defined by a set of discriminant functions, one for every dimension in the optimal space. In this study, the discriminant functions were estimated from the training dataset, and classification of new data was performed based on the minimum distance of the new data sample to the centroids of each group in the discriminant space. One disadvantage with LDA, however, is that features

not relevant for classification can be unnecessarily included in the discriminant functions.

To overcome this limitation, LDA can be applied in a stepwise manner [stepwise LDA (SLDA)].[10,31] In SLDA, the feature with the maximum discriminating power is first selected. This feature is then combined with the remaining features, one at a time, to find the combination with largest discriminating power. The process is continued until the addition of a new feature does not increase the discriminating power. It should be noted that SLDA does not warranty that the final feature combination would be superior to other possible ones. There are several available criteria for entering or removing new variables at each step: Wilks' lambda, unexplained variance, Mahalanobis' distance, and smallest F ratio. In this study, the Mahalanobis' distance criterion with a partial F test (α=0.15) was adopted to sequentially incorporate features.

Principal component analysis (PCA)[10,11,32] also transforms the original feature space into a smaller set of linear combinations of the original variables. Although PCA may not provide direct insight into the biochemical basis of tissue fluorescence, this method condenses the spectroscopic information into a few manageable components, with minimal information loss. In PCA, the eigenvectors and the eigenvalues from the covariance matrix of the feature vector are estimated. By ordering the eigenvectors in descending order of the eigenvalues (largest first), one can create an ordered orthogonal basis with the first eigenvector having the direction of largest variance of the data. In this way, we can find directions in which the feature set has the most significant amounts of information. Projection of the original feature vectors into each of these directions will define a new independent variable called a principal component or factor. Since each factor accounts for a certain percentage of the variation in the original features, only a subset of factors accounting for most of the variation is considered for classification. In this study, PCA was applied to the original feature space, and LDA was applied to the reduced space defined by the principal components.

2.7.2 *Nonlinear classification algorithm*

Artificial neural networks have been successfully used in many classification problems.[12,13,31] The most commonly used neural network architecture is the feed-forward neural network (FFNN) with an input layer, an output layer, and multiple hidden layers. Under FFNN configuration, each layer is connected only to the subsequent layer by variable weights, which are adjusted to minimize a cost function (classification accuracy) using an optimization algorithm. In this study, a FFNN with a single hidden layer and a Levenberg-Marquardt optimization approach[31] was developed.

2.7.3 *Classification performance analysis*

Estimation of the expected performance of a classifier is an important yet difficult problem in pattern recognition. A number of testing procedures have been proposed and are widely used. In the holdout method, a number of the original samples are withheld from the design process. This provides an independent test set, but drastically reduces the size of the training set. In the resubstitution method, the classifier is tested on the original training samples. This maintains the size of the training set, but ignores the independence issue, generating a dangerously optimistic performance estimate. The leave-one-out method is designed to alleviate these difficulties. In the leave-one-out method, one sample is excluded from the database and the classifier is trained with the remaining samples. It avoids drastically dividing the available sample set into training and test, while maintaining independence between them. Thus, the procedure utilizes all available samples more efficiently, and produces a conservative error estimate.

One of the goals of the present study was to investigate whether spectral information alone or a combination of spectral and time-resolved information were needed for lesion classification. Therefore, three types of spectroscopic feature were independently used to develop each of the classification algorithms described before: 1. SP alone, 2. a combination of SP-LAG, and 3. a combination of SP-BEXP. The classification results were tested using the leave-one-out approach. Values of sensitivity (SE) and specificity (SP) were reported for each combination of classifier (LDA, SLDA, PCA, FFNN) and feature type (SP, SP-LAG, SP-BEXP).

3 Results

3.1 *Histology*

A total of 73 sections of aorta (eight rabbits) were investigated *in vivo*. Out of these, 26 sections corresponded to normal aorta and 47 sections to atherosclerotic lesions. The lesions were divided as thin-collagen (N=10), thin-mac (N=7), thick-collagen (N=16), and thick-mac (N=14).

3.2 *Time-Resolved Fluorescence Spectra*

Representative time-resolved fluorescence spectra are shown in Fig. 1 (left panels). All spectra presented a main peak at ~385 to 395 nm. A secondary peak was observed at ~440 to 450 nm. The peak intensity values of the latter were found as being tissue-type dependent, as they were the corresponding decay rate. The corresponding measured and estimated decays at 390 nm (right panels) and the normalized error (NErr) as retrieved by LDT are shown in Fig. 1 (right panels). NErr values were <5% of the peak fluorescence amplitude and randomly distributed around zero. The autocorrelation function of the residuals did not present low-frequency oscillations characteristic of nonrandom residuals, and was mostly contained within the 95% confidence interval for random independent time series (dotted lines). These observations indicate excellent fit between the measured and estimated fluorescence decays, showing that the fluorescence FIRFs were properly estimated using LDT.

3.3 *Spectroscopic Parameters*

The group values (mean ± SE) of the spectroscopic parameters along the emission wavelengths are depicted in Fig. 2.

3.3.1 *Steady-state spectral parameters*

The normalized steady-state spectrum [Fig. 2(a)] presented a relatively broadband emission (a main peak at ~385 to 395 nm and a second peak at ~440 to 450 nm) and a valley at 415 nm. The valley corresponds to the hemoglobin absorption as previously reported.[8] The broadest band emission spectrum corresponded to the normal and thin-collagen

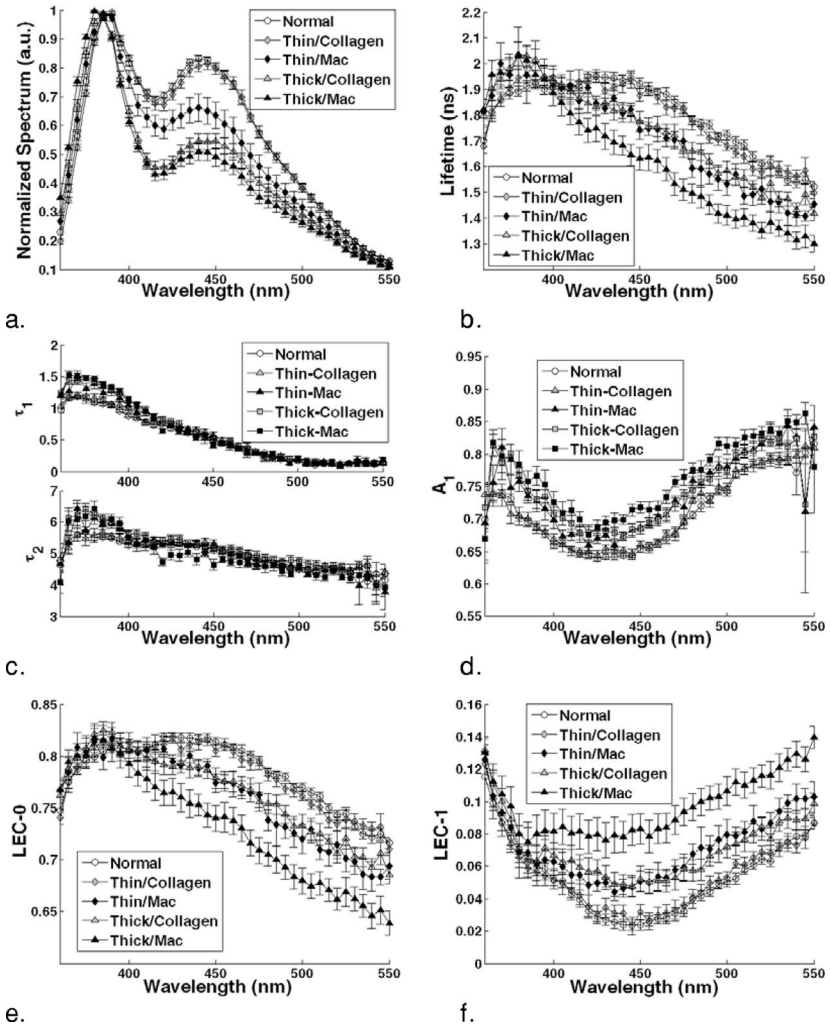

Fig. 2 Group values (mean ± SE) of the spectroscopic parameters along the emission wavelengths: (a) normalized spectrum, (b) lifetimes, and Laguerre coefficients (c) LEC-0 and (d) LEC-1.

samples, with the highest peak at ~450 nm (~80% of the main peak). The emission intensity of the thin-mac subgroup at 440 nm averaged ~65% of the main peak intensity. The emission of the thick lesions was narrower, presenting the lowest intensities values at ~450 nm (~50% of the main peak). These results suggest that the relative intensity at ~450 nm may provide information for discriminating normal and thin-collagen lesions from thin-mac and thick lesions.

3.3.2 *Conventional time-resolved parameters*

The average radiative lifetime values [Fig. 2(b)] diminished gradually with the increasing λ_E (>400 nm). The lifetime decrease rate was found to be tissue-type dependent. The thick-mac subgroup was characterized by the shortest lifetime values and the steepest decrease of lifetime with increasing λ_E. It was followed by the thin-mac and thick-collagen samples, and by the normal and thin-collagen samples. These results indicate that the lifetime values at longer wavelengths (>440 nm) may provide information for discriminating normal and thin-collagen lesions from thin-mac and thick-collagen, and these from thick-mac lesions.

The biexponential time constant τ_1 also decreased with increasing λ_E [Fig. 2(c), top panel]. Values of τ_1 at shorter wavelengths (below 400 nm) provided information for discriminating normal and thin-collagen from thin-mac and thick samples. The time constant τ_2 presented very similar distribution to τ_1 [Fig. 2(c), bottom panel]. However, between ~420 and 450 nm, τ_2 values from the thick-mac samples presented shorter values than those from the other groups. The relative amplitude A_1 at wavelengths between 390 and 450 nm provided information for discriminating normal and thin-collagen samples from thin-mac and thick-collagen samples, and thick-mac samples from the other groups [Fig. 2(d)]. Estimation of τ_2 and A_1 became less accurate at wavelengths above 530 nm, as is evident by the large error bars.

3.3.3 *Laguerre expansion coefficients*

The Laguerre expansion coefficient of zero order (LEC-0) presented a similar distribution to that of average lifetimes [Fig. 2(e)]. The LEC-1 coefficients [Fig. 2(f)] revealed opposite trends to the LEC-0 coefficients, decreasing with λ_E until 450 nm, before increasing afterward. The minimal variation

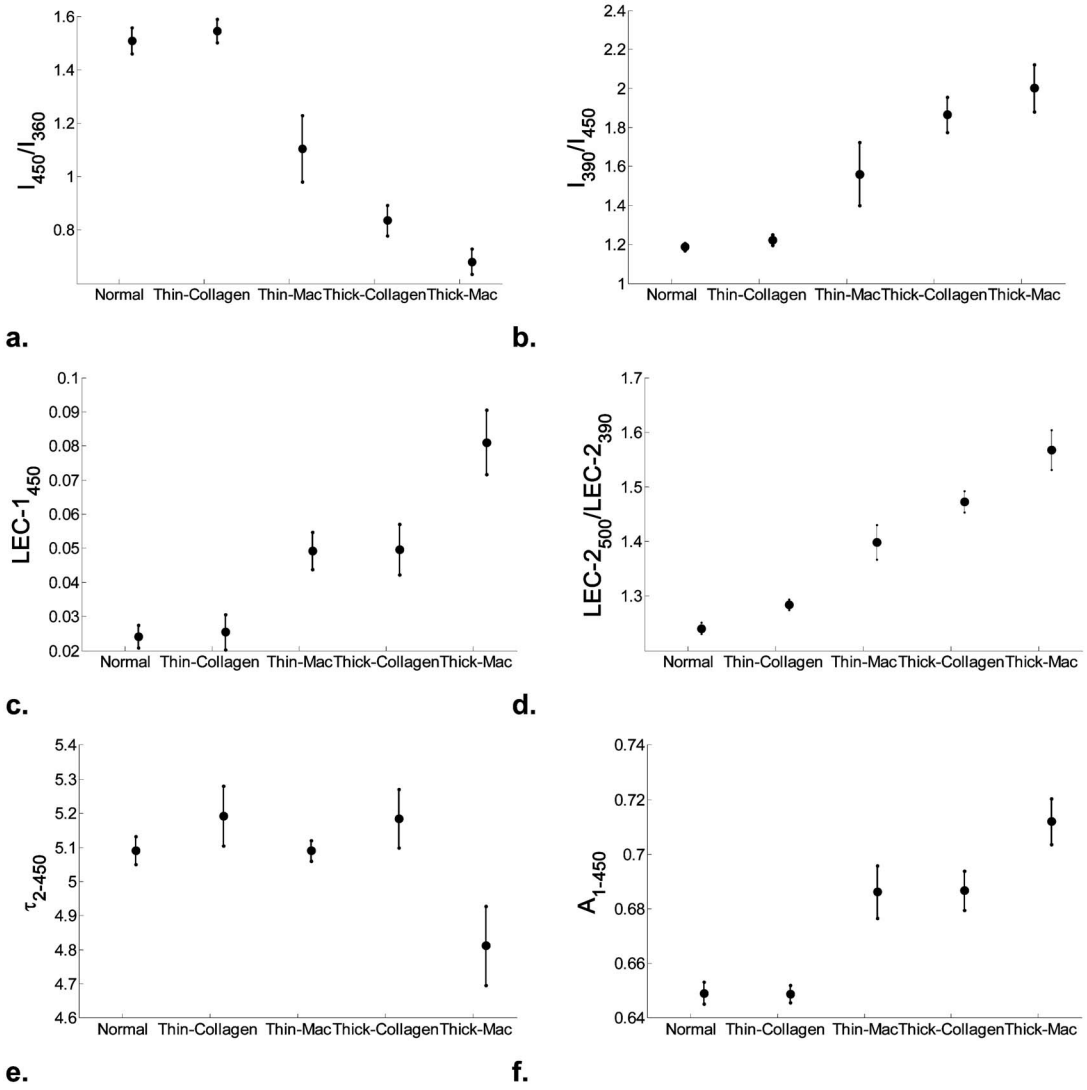

Fig. 3 Results of the statistical analysis (mean ± SE) of the main spectral and time-resolved (Laguerre and bi-exponential) parameters.

of LEC-1 with wavelength was observed for the thick-mac samples. Both LEC-0 and LEC-1 above 450 nm provided information for discriminating normal and thin-collagen samples from thin-mac and thick-collagen lesions, and these from thick-mac lesions.

3.4 *Statistical Analysis*

The results of the statistical analysis (mean ± SE) of the main spectroscopic parameters providing discriminant information among distinct types of tissues are depicted in Fig. 3. The statistical analysis indicated that spectral parameters such as the ratios of intensities at a few emission wavelengths (360, 390, and 450 nm) provided information for discriminating normal and thin-collagen lesions from thin-mac and thick lesions. For example, the ratios of emission intensities at 450 nm over 360 nm (I_{450}/I_{360}) from the normal and thin-collagen groups were both significantly larger than those from the other groups. More interesting, the ratio I_{450}/I_{360} from the thick lesions was significantly smaller than those from the other tissue types [Fig. 3(a)]. The opposite was found for I_{390}/I_{450} [Fig. 3(b)].

The statistical analysis also indicates that time-resolved parameters such as the Laguerre expansion coefficients at a few emission wavelengths (390, 450, and 500 nm) and their ratios provide information to discriminate the tissues in question. The LEC-1 at 450 nm ($LEC-1_{450}$) from the thick-mac group was significantly larger than those from the other groups [Fig. 3(c)]. More interesting, the ratio of $LEC-2_{500}/LEC-2_{390}$ was significantly different for every group, except for the normal and thin-collagen samples [Fig. 3(d)]. The biexponential parameters at 390 and 450 nm were also different among tissue types. The τ_2 at 450 nm (τ_{2-450}) was significantly smaller for the thick-mac lesions, relative to the collagen lesions [Fig. 3(e)]. The relative amplitude A_{1-450} was significantly smaller for the normal and thin-collagen group, and larger for the thick-mac group, with respect to the thin-mac and thick-collagen lesions [Fig. 3(f)]. Table 1 summarizes the values of the main spectral and time-resolved parameters used for classification.

Table 1 Representative set of spectroscopic parameters that allows for tissue subgroup discrimination.

	N-athero	Thin-collagen	Thin-macrophage	Thick-collagen	Thick-macrophage
I_{450}/I_{360}	1.51±0.05	1.55±0.04	1.10±0.12	0.84±0.06	0.68±0.05
I_{390}/I_{450}	1.19±0.02	1.22±0.03	1.56±0.16	1.86±0.09	2.00±0.12
$LEC-1_{450}$	0.024±0.003	0.026±0.005	0.049±0.005	0.049±0.007	0.081±0.009
$LEC-2_{500}/LEC-2_{390}$	1.24±0.01	1.28±0.01	1.40±0.03	1.47±0.02	1.57±0.04
τ_{2-450}	5.09±0.04	5.19±0.09	5.09±0.03	5.18±0.09	4.81±0.12
A_{1-450}	0.65±0.004	0.65±0.003	0.69±0.009	0.69±0.007	0.71±0.004

3.5 *Classification*

Classification 1 was designed to separate normal, thick-collagen, and thick-mac subgroups. The classification results are summarized in Table 2. Based on the statistical analysis, a total of five SP, 14 LAG, and six BEXP features were selected for developing the classification algorithms. LDA and FFNN used the complete sets of features, while SLDA selected three SP, eight LAG, and six BEXP features. In the PCA classification, a total of five SP, six LAG, and six BEXP principal components were used. Classification with only SP parameters discriminated normal from thick lesions, but not thick-collagen from the thick-mac lesions. Classification with combined SP and time-resolved features (either LAG or BEXP parameters) discriminated the three groups from each other. There was no significant difference in using the LAG or the BEXP features in terms of classification performance (86.5 and 87.6%, respectively). The comparison among the different classification algorithms [Table 2 and Fig. 4(a)] showed that for our data, SLDA and PCA approaches provided the best performance (86.7 and 86.3%, respectively), followed by LDA and FFNN (81.5 and 78.2%, respectively).

The classification based on SLDA provided the best performance (92.9%). Figures 4(b) through 4(d) depict samples of the three representative groups and the corresponding means in the space spanned by the two discriminant functions. For the case of the SP-based classification [Fig. 4(b)], the normal samples were discriminated from the thick samples (SE$>$90%, SP 100%); however, the thick-collagen and thick-mac samples were not classified correctly (SE$<$65%). For the case of the SP-LAG-based classification [Fig. 4(c)], the normal samples were also separated from the thick samples (SE$>$96%, SP 100%). More important, the thick-collagen samples were also discriminated from the thick-mac samples (SE$>$93%, SP$>$95%). Similar results were observed for the SP-BEXP-based classification [Fig. 4(d)].

Classification 2 targeted the discrimination of normal, thin-collagen, and thin—mac samples using the best-performed SLDA and PCA algorithms. The classification results are summarized in Table 3. The classification based on only SP parameters did not allow discrimination of any of the groups. The classification using both SP and TR features (either LAG or BEXP parameters) facilitated discrimination of most of the

Table 2 First classification results: normal/thin versus thick-collagen versus thick-mac.

Feature	Sample	LDA		SLDA		PCA		FFNN	
		SE	SP	SE	SP	SE	SP	SE	SP
Spectral	Normal/thin	92.3	100	92.3	100	96.1	100	95.4	95.3
	Thick-collagen	62.5	87.5	62.5	87.5	62.5	82.5	52.5	85.0
	Thick-mac	64.3	80.9	64.3	80.9	57.1	85.7	51.4	80.5
Spectral Laguerre	Normal/thin	92.3	96.7	96.2	100	92.3	100	92.3	96.7
	Thick-collagen	81.3	87.5	93.8	95.0	93.8	92.5	76.3	85.0
	Thick-mac	64.3	90.5	85.7	95.2	85.7	95.2	61.4	90.0
Spectral Bi-Exp	Normal/thin	96.2	100	100	100	100	100	96.9	98.7
	Thick-collagen	81.3	90.0	87.5	92.5	87.5	92.5	71.3	88.0
	Thick-mac	71.4	90.5	78.6	95.2	78.6	95.2	68.6	89.1

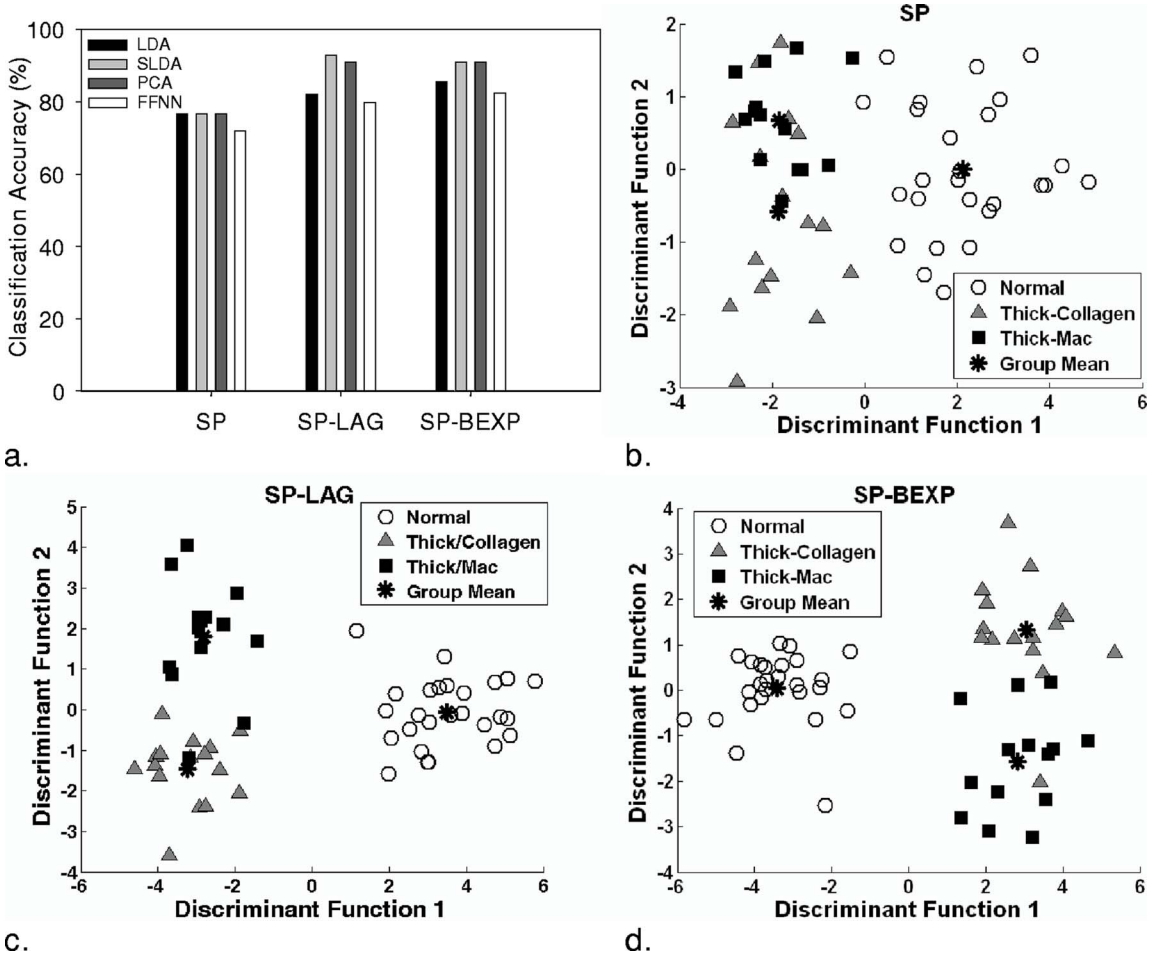

Fig. 4 First classification results (normal versus thick-collagen versus thick-mac): (a) classification performance for the different feature types (SP, SP-LAG, SP-BEXP) and algorithms (LDA, SLDA, PCA, FFNN); and sample maps in the discriminant function domain from the SLDA classification with (b) SP, (c) SP-LAG, and (d) SP-BEXP features.

thin-mac samples (SE > 85%, SP > 94%), but did not allow discrimination of normal and thin-collagen samples from each other. The classification performance based on LAG (67.5%) was similar with that based on BEXP features (66.3%).

As shown in Fig. 5(a), the SLDA performed better than PCA (69 and 62%, respectively). The classification with the SLDA algorithm is shown in Figs. 5(b), 5(c), and 5(d). In the case of SP-based classification [Fig. 5(b)] none of the groups were discriminated. While in the case of SP-LAG and SP-BEXP [Figs. 5(c) and 5(d)], the thin-mac samples were separated from normal and thin-collagen samples. It is important to note that only seven thin-mac samples were available for this analysis; thus these results need to be carefully interpreted.

4 Discussion

4.1 *Laguerre Deconvolution Technique as a Method for Analysis of Time-Resolved Laser-Induced Spectroscopy Data from Tissue*

Our results demonstrated that the Laguerre deconvolution technique represents an accurate and robust approach for the analysis of TR-LIFS data. The technique was able to estimate the FIRF of a variety of arterial samples presenting distinct

Table 3 Second classification results: normal versus thin-collagen versus thin-mac.

Feature	Sample	SLDA		PCA	
		SE	SP	SE	SP
Spectral	Normal	65.4	88.2	57.7	88.2
	Thin-collagen	80.0	63.6	70.0	66.7
	Thin-mac	42.9	97.2	57.1	88.9
Laguerre	Normal	69.2	76.5	61.5	64.7
	Thin-collagen	70.0	81.8	60.0	72.7
	Thin-mac	85.7	94.4	71.4	97.2
Bi-Exp	Normal	69.2	70.6	61.5	70.6
	Thin-collagen	60.0	75.8	60.0	72.7
	Thin-mac	85.7	100	71.4	94.4

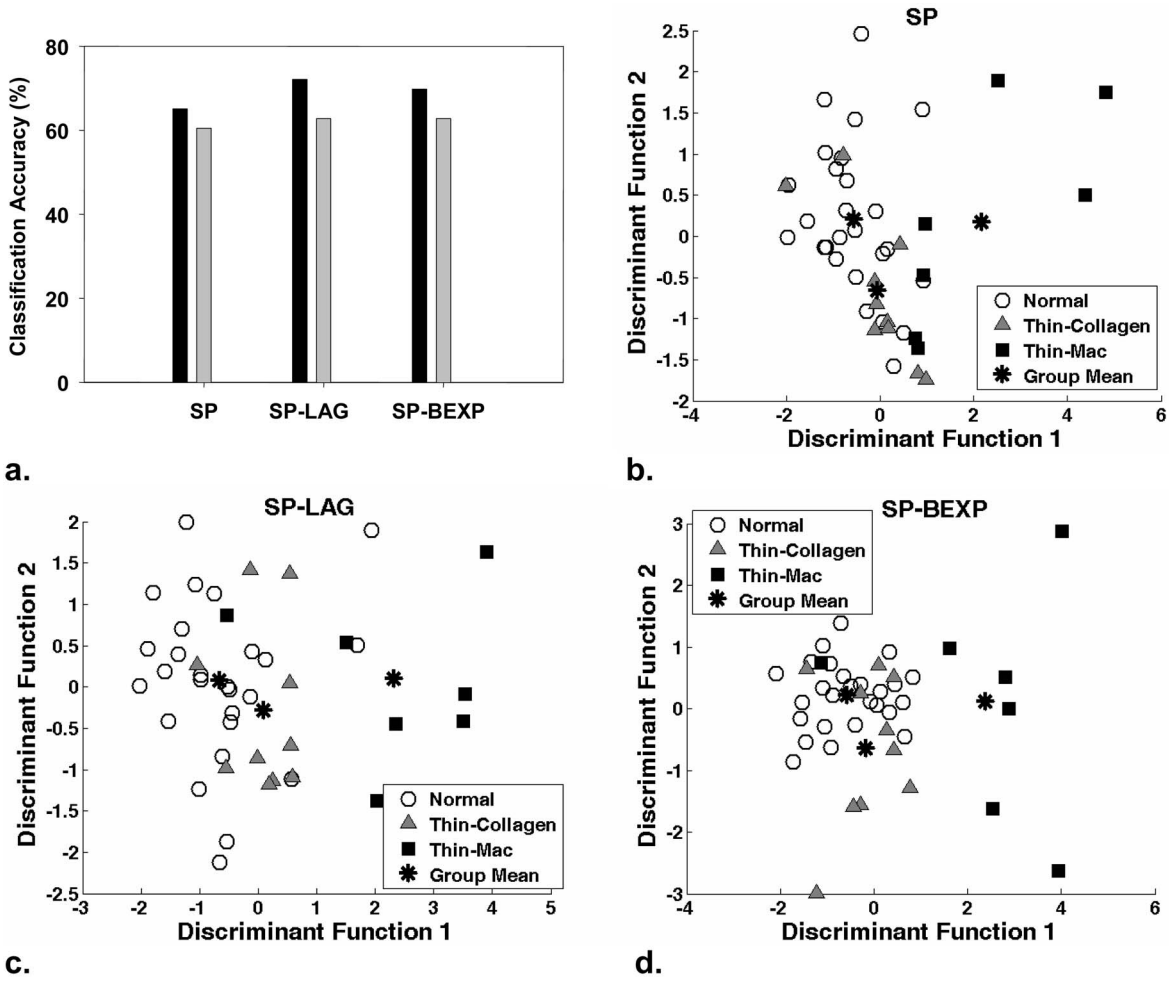

Fig. 5 Second classification results (normal versus thin-collagen versus thin-mac): (a) classification performance for the different feature types (SP, SP-LAG, SP-BEXP) and algorithms (SLDA in black, PCA in gray); and sample maps in the discriminant function domain from the SLDA classification with (b) SP, (c) SP-LAG, and (d) SP-BEXP features.

biochemical compositions with good precision (NErr $<5\%$). An important observation was that the estimation of the conventional biexponential parameters at wavelengths above 530 nm became less accurate as the signal-to-noise ratio decreased [error bars in Figs. 2(e) and 2(f)], while the estimation based on Laguerre expansion coefficients remained unaffected [error bars in Figs. 2(e) and 2(f)]. This suggests that the Laguerre deconvolution technique represents a more robust method for TR-LIFS data analysis than the conventional iterative multiexponential method.

The traditional multiexponential technique involves the estimation of intrinsic nonlinear parameters (the decay constants), which requires more complex and computationally expensive nonlinear least-square iterative approaches.[30] Although single exponential fitting can be linearized via logarithmic transformation, complex fluorescence systems containing more than one fluorophore cannot be accurately modeled with a single decay. An alternative for fitting complex decays is the stretched exponential method, which also allows for fast convergence. One drawback of this approach, however, is that curve fitting instead of actual deconvolution is usually applied. In the Laguerre deconvolution technique, the problem of deconvolving the system response and estimating the FIRF is reduced to finding the expansion coefficients of an overdetermined system of linear equations [Eq. (5)] via the linear least-square minimization approach.[9,29] Such a linearization of the convolution equation via an orthonormal expansion allows fast and robust TR-LIFS data deconvolution. These specific advantages of the Laguerre method become even more important in the context of TR-LIFS-based *in-vivo* tissue diagnosis, where the quality of the signal cannot always be warranted and the speed of data analysis is of crucial importance.

4.2 *Laguerre Expansion Coefficients as New Means for Characterizing the Time-Resolved Laser-Induced Spectroscopy Data*

It was observed that the Laguerre expansion coefficients (LEC) were highly correlated with the intrinsic lifetime values (especially LEC-0), suggesting that the LECs describe the dynamics of the fluorescence intensity decay.[9] This can be explained by the orthogonality of the Laguerre basis, which implies that the value of each LEC depends exclusively on the fluorescence decays to be fitted.[18,30] The fluorescence time-decay characteristics captured by the LECs also reflect the

biochemical composition of the artery. The normal and thin-collagen groups presented constant lifetimes values (~1.9 ns) along the emission spectra (370 to 450 nm), suggesting that their fluorescence emission is dominated by elastin, characterized by a fairly constant lifetime value of ~2 ns between ~360 and 500 nm.[1,8] The thick lesions presented slightly longer but decreasing lifetimes (~2 ns) at increasing wavelengths, similar to the lifetime-wavelength dependency found in collagen.[1,8] The LEC-0 presented the same tissue dependency variation as the lifetime values, indicating that this coefficient captures the average fluorescence time-decay characteristics of the tissue.

Lipid components exhibit shorter-lived emission when compared to the structural proteins of elastin or collagen.[1,8] This was consistent with our results showing a significant decrease in lifetime in the lesion rich in macrophages relative to those rich in collagen. Also, a large normalized LEC-1 is characteristic of a faster FIRF decay.[9] Thus, lipids should also present large LEC-1 values. This was reflected in the thick-mac samples, which were characterized by the largest LEC-1 and provided the best discrimination of the thick-mac group [Figs. 2(f) and 3(c)]. This particular result indicates that important characteristics of the fluorescence decay shape, not reflected on their conventional lifetime values, can be captured by the higher-order Laguerre expansion coefficients. All these results taken together demonstrate that Laguerre expansion coefficients offer a new domain for representing time-resolve information in a very compact, accurate, complete, and computationally efficient way.

4.3 *Feature Selection*

The results of the statistical analysis showed that TR-LIFS information most relevant for discriminating atherosclerotic lesions was concentrated at a few number of emission wavelengths (360, 390, 450, and 500 nm), confirming previous observations.[10,12] This indicates that it is no longer necessary to acquire the complete time-resolved fluorescence spectrum, but only the fluorescence at a reduced number of emission wavelengths. Consequently, the acquisition time could be reduced significantly, thus facilitating the real-time diagnostics of atherosclerotic plaque. We hypothesize that similar concentrations of discriminant information in a reduced number of emission wavelengths might be found in other biological tissue and biochemical systems, as it has been suggested elsewhere.[2,4,6]

4.4 *Classification*

Although in this study we used a small database, our results indicate that classification algorithms derived from the Laguerre expansion coefficients are robust enough to allow good detection of macrophage infiltration in arterial intima (~70% for thin-foam and ~93% for thick-foam lesions). Moreover, the classification accuracy could be further improved once the number of samples for each tissue type in the training set increases. It was also observed that features from the steady-state fluorescence spectrum can discriminate a normal artery from more advanced thick lesions. However, they cannot detect the presence of macrophages. On the other hand, by incorporating features related to the fluorescence time-decay characteristics of the artery (i.e., LECs or biexponential parameters), it is possible not only to improve the detection of advanced (thick) lesions, but also to discriminate lesions with macrophages infiltration. Thus, our results showed that time-resolved fluorescence information derived from the LECs can be used to develop TR-LIFS-based tissue diagnosis methods, and specifically to detect macrophage infiltration in atherosclerotic plaques, an important predictor of plaque rupture.

It was also observed that classifications with either LECs or biexponential parameters provided similar performance. One important advantage of LDT over the multiexponential approach, however, is that the former performs significantly faster. This would be of special importance in the context of real-time tissue diagnosis using fluorescence lifetime imaging (FLIM), where conventional methods of analysis are time consuming, making it almost impossible to allow real-time applications.[33] The LDT technique can be easily adapted for FLIM analysis[34] and, combined with proper classification algorithms, has the potential for imaging features of plaque vulnerability (such as the presence of macrophages) and other interesting tissue pathologies in real time.

The use of redundant features may generate a classifier that is specifically designed to discriminate the training set and may unduly weight less distinct features.[10,12,31] This could result in a discriminant function with decreased ability to classify new samples. Such outcome was observed in the LDA and FFNN algorithms, which use all the features available. In contrast, SLDA and PCA, which use a reduced but more selected group of features, provided the best classification performance. One possible additional explanation of the poor performance of the FFNN approach is that the number of parameters to be estimated is much larger, thus demanding a larger number of training samples. These results also support the empiric observation that the differences in the fluorescence emission of the various types of atherosclerotic lesions are manifested in a reduced number of spectral and TR features.[10,12]

Another interesting observation was that all four algorithms correctly classified most of the normal samples (~96%), while the classification accuracy of atherosclerotic samples was lower (~90%). This is explained by the greater heterogeneity of atherosclerotic lesions relative to normal aorta. In the present study, lesions were characterized based on their intima plaque thickness and their relative collagen/macrophage contents. Because atherosclerosis is a progressive disease, the lesions are quite heterogeneous and present a large variability in their morphology and biochemical composition.[17] Thus, a histopathological categorization of the lesions (the gold standard for the development of our TR-LIFS classifiers) can by itself be difficult to define. This might explain the difficulty on classifying different types of atherosclerotic lesions, as compared to normal arterial walls. Thus, a more comprehensive classification of the plaques based on their histopathological, morphological, and biochemical characteristics should help to improve the diagnosis capability of TR-LIFS.

5 Conclusion

We have demonstrated that the Laguerre deconvolution method applied to *in-vivo* TR-LIFS measurements provides accurate FIRF estimation of normal and atherosclerotic arter-

ies. In addition, the Laguerre expansion coefficients can be used to characterize the arterial tissue and to detect changes in its biochemical composition. This study also indicates that, although steady-state characteristics can be used to separate normal and early lesions from more advanced lesions, time-resolved properties are essential for detecting macrophages in the arterial wall. Since discriminate information is concentrated in a few emission wavelengths, it is no longer necessary to acquire the entire emission spectrum. Thus, the acquisition time can be reduced, facilitating the development of real-time diagnostic methods. Although classification with both Laguerre and multiexponential parameters show similar performance, the Laguerre approach is faster and more robust, and can be easily extended to imaging analysis. Finally, our results indicate that classification algorithms (SLDA and PCA) that use a reduced but selected number of features yield the best performance in tissue classification. In summary, this study demonstrates the potential of using TR information, by means of Laguerre expansion coefficients, for *in-vivo* fluorescence-based tissue characterization and diagnosis, and specifically for the detection of macrophages infiltration in atherosclerotic lesions, a key predictor for plaque rupture.

Acknowledgment

This work was supported by the National Institutes of Health grant R01 HL 67377.

References

1. L. Marcu, M. C. Fishbein, J. M. Maarek, and W. S. Grundfest, "Discrimination of human coronary artery atherosclerotic lipid-rich lesions by time-resolved laser-induced fluorescence spectroscopy," *Arterioscler., Thromb., Vasc. Biol.* **21**, 1244–1250 (2001).
2. D. Goujon, M. Zellweger, A. Radu, P. Grosjean, B. C. Weber, B. H. van den, P. Monnier, and G. Wagnieres, "In vivo autofluorescence imaging of early cancers in the human tracheobronchial tree with a spectrally optimized system," *J. Biomed. Opt.* **8**(1), 17–25 (Jan. 2003).
3. S. Lam, T. Kennedy, M. Unger, Y. E. Miller, D. Gelmont, V. Rusch, B. Gipe, D. Howard, J. C. LeRiche, A. Coldman, and A. F. Gazdar, "Localization of bronchial intraepithelial neoplastic lesions by fluorescence bronchoscopy," *Chest* **113**(3), 696–702 (Mar. 1998).
4. W. C. Lin, S. A. Toms, M. Motamedi, E. D. Jansen, and A. Mahadevan-Jansen, "Brain tumor demarcation using optical spectroscopy; an in vitro study," *J. Biomed. Opt.* **5**(2), 214–220 (Apr. 2000).
5. W. C. Lin, S. A. Toms, M. Johnson, E. D. Jansen, and A. Mahadevan-Jansen, "In vivo brain tumor demarcation using optical spectroscopy," *Photochem. Photobiol.* **73**(4), 396–402 (Apr. 2001).
6. M. F. Mitchell, S. B. Cantor, N. Ramanujam, G. Tortolero-Luna, and R. Richards-Kortum, "Fluorescence spectroscopy for diagnosis of squamous intraepithelial lesions of the cervix," *Obstet. Gynecol. (N.Y., NY, U. S.)* **93**(3), 462–470 (Mar. 1999).
7. M. Panjehpour, C. E. Julius, M. N. Phan, T. Vo-Dinh, and S. Overholt, "Laser-induced fluorescence spectroscopy for in vivo diagnosis of non-melanoma skin cancers," *Lasers Surg. Med.* **31**(5), 367–373 (2002).
8. L. Marcu, W. S. Grundfest, and M. C. Fishbein, "Time-resolved laser-induced fluorescence spectroscopy for staging atherosclerotic lesions," in *Handbook of Biomedical Fluorescence*, Chap. 12, M. A. Mycek and B. W. Pogue, Eds., Marcel Dekker, New York (2003).
9. J. A. Jo, Q. Fang, T. Papaioannou, and L. Marcu, "Fast nonparametric deconvolution of fluorescence decay for analysis of biological systems," *J. Biomed. Opt.* **9**(4), 743–752 (2004).
10. K. M. O'Brien, A. F. Gmitro, G. R. Gindi, M. L. Stetz, F. Cutruzzola, L. I. Laifer, and L. I. Deckelbaum, "Development and evaluation of spectral classification algorithms for fluorescence guided laser angiograph," *IEEE Trans. Biomed. Eng.* **36**, 424–431 (1989).
11. N. Ramanujam, M. F. Mitchell, A. Mahadevan, S. Thomsen, A. Malpica, T. Wright, N. Atkinson, and R. Richards-Kortum, "Development of a multivariate statistical algorithm to analyze human cervical tissue fluorescence spectra acquired in vivo," *Lasers Surg. Med.* **19**(1), 46–62 (1996).
12. G. R. Gindi, C. J. Darken, K. M. O'Brien, M. L. Stetz, and L. I. Deckelbaum, "Neural network and conventional classifiers for fluorescence-guided laser angioplasty," *IEEE Trans. Biomed. Eng.* **38**, 246–252 (1991).
13. G. A. Rovithakis, M. Maniadakis, M. Zervakis, G. Filippidis, G. Zacharakis, A. N. Katsamouris, and T. G. Papazoglou, "Artificial neural networks for discriminating pathologic from normal peripheral vascular tissue," *IEEE Trans. Biomed. Eng.* **48**(10), 1088–1097 (Oct. 2001).
14. K. Tumer, N. Ramanujam, J. Ghosh, and R. Richards-Kortum, "Ensembles of radial basis function networks for spectroscopic detection of cervical precancer," *IEEE Trans. Biomed. Eng.* **45**(8), 953–961 (Aug. 1998).
15. W. Lin, X. Yuan, P. Yuen, W. I. Wei, J. Sham, P. Shi, and J. Qu, "Classification of in vivo autofluorescence spectra using support vector machines," *J. Biomed. Opt.* **9**(1), 180–186 (Jan. 2004).
16. E. Falk, P. K. Shah, and V. Fuster, "Coronary plaque disruption," *Circulation* **92**, 657–671 (1995).
17. M. Naghavi, P. Libby, E. Falk, S. W. Casscells, S. Litovsky, J. Rumberger, J. J. Badimon, C. Stefanadis, P. Moreno, G. Pasterkamp, Z. Fayad, P. H. Stone, S. Waxman, P. Raggi, M. Madjid, A. Zarrabi, A. Burke, C. Yuan, P. J. Fitzgerald, D. S. Siscovick, C. L. de Korte, M. Aikawa, K. E. Juhani Airaksinen, G. Assmann, C. R. Becker, J. H. Chesebro, A. Farb, Z. S. Galis, C. Jackson, I. K. Jang, W. Koenig, R. A. Lodder, K. March, J. Demirovic, M. Navab, S. G. Priori, M. D. Rekhter, R. Bahr, S. M. Grundy, R. Mehran, A. Colombo, E. Boerwinkle, C. Ballantyne, W. Insull Jr., R. S. Schwartz, R. Vogel, P. W. Serruys, G. K. Hansson, D. P. Faxon, S. Kaul, H. Drexler, P. Greenland, J. E. Muller, R. Virmani, P. M. Ridker, D. P. Zipes, P. K. Shah, and J. T. Willerson, "From vulnerable plaque to vulnerable patient: a call for new definitions and risk assessment strategies: Part I," *Circulation* **108**, 1664–1672 (2003).
18. P. Libby, P. M. Ridker, and A. Maseri, "Inflammation and atherosclerosis," *Circulation* **105**, 1135–1143 (2002).
19. D. Steinberg, "Atherogenesis in perspective: hypercholesterolemia and inflammation as partners in crime," *Nat. Med.* **8**, 1211–1217 (2002).
20. P. R. Moreno, E. Falk, I. F. Palacios, J. B. Newell, V. Fuster, and J. T. Fallon, "Macrophage infiltration in acute coronary syndromes. Implications for plaque rupture," *Circulation* **90**, 775–778 (1994).
21. G. J. Tearney, H. Yabushita, S. L. Houser, H. T. Aretz, I. K. Jang, K. H. Schlendorf, C. R. Kauffman, M. Shishkov, F. F. Halpern, and B. E. Bouma, "Quantification of macrophage content in atherosclerotic plaques by optical coherence tomography," *Circulation* **107**, 113–119 (2003).
22. A. Christov, E. Dai, M. Drangova, L. Liu, G. S. Abela, P. Nash, G. McFadden, and A. Lucas, "Optical detection of triggered atherosclerotic plaque disruption by fluorescence emission analysis," *Photochem. Photobiol.* **72**, 242–252 (2000).
23. K. Arakawa, K. Isoda, T. Ito, K. Nakajima, T. Shibuya, and F. Ohsuzu, "Fluorescence analysis of biochemical constituents identifies atherosclerotic plaque with a thin fibrous cap," *Arterioscler., Thromb., Vasc. Biol.* **22**, 1002–1007 (2002).
24. L. Marcu, J. A. Jo, Q. Fang, T. Papaioannou, A. Dorafshar, T. Reil, J. H. Qiao, D. Baker, M. C. Fishbein, and J. A. Freischlag, "*In-vivo* detection of macrophages in a rabbit atherosclerotic model by time-resolved laser-induced fluorescence spectroscopy," *Atherosclerosis* **181**, 295–303 (2005).
25. T. Papaioannou, Q. Fang, J. A. Jo, R. Vaitha, A. Dorafshar, T. Reil, J. Qian, M. C. Fishbein, J. Freischlag, and L. Marcu, "Validation of a time-resolved fluorescence spectroscopy apparatus: spectral-resolved fluorescence lifetime and fluorescence photobleaching of rabbit arterial wall, in-vivo and ex-vivo investigations," (to be published).
26. Q. Fang, T. Papaioannou, J. A. Jo, R. Vaitha, K. Shastry, and L. Marcu, "Time-domain laser-induced fluorescence spectroscopy apparatus for clinical diagnostics," *Rev. Sci. Instrum.* **75**, 151–162 (2004).
27. L. Marcu, W. S. Grundfest, and J. M. Maarek, "Photobleaching of arterial fluorescent compounds: characterization of elastin, collagen and cholesterol time-resolved spectra during prolonged ultraviolet irradiation," *Photochem. Photobiol.* **69**, 713–721 (1999).
28. J. M. Maarek, L. Marcu, W. J. Snyder, and W. S. Grundfest, "Time-resolved fluorescence spectra of arterial fluorescence compounds: re-

construction with Laguerre expansion technique," *Photochem. Photobiol.* **71**, 178–187 (2000).
29. V. Z. Marmarelis, "Identification of nonlinear biological systems using Laguerre expansion of kernels," *Ann. Biomed. Eng.* **21**, 573–589 (1993).
30. J. R. Lakowicz, *Principles of Fluorescence Spectroscopy*, 2nd ed., Kluwer Academic/Plenum, New York (1999).
31. R. O. Duda, P. E. Hart, and D. G. Stork, *Pattern Classification*, John Wiley and Sons, New York (2004).
32. R. Kramer, *Chemometric Techniques for Quantitative Analysis*, Marcel Dekker, New York (1998).
33. R. Cubeddu, D. Comelli, C. D'Andrea, P. Taroni, and G. Valentini, "Time-resolved fluorescence imaging in biology and medicine," *J. Phys. D* **35**, R61–R76 (2002).
34. J. A. Jo, Q. Fang, T. Papaioannou, and L. Marcu, "Ultra-fast method for the analysis of fluorescense lifetime imaging microscopy based on the Laguerre expansion technique," *IEEE J. Sel. Top. Quantum Electron.* **11**, 835–845 (2005).